J. Fluid Mech. (2007), *vol.* 582, *pp.* 153–168.
doi:10.1017/S0022112007006209 Printed in the United Kingdom

Energy-minimizing kinematics in hovering insect flight

GORDON J. BERMAN[1] AND Z. JANE WANG[2]

[1]Cornell University, Department of Physics, Ithaca, NY 14853, USA

[2]Cornell University, Department of Theoretical and Applied Mechanics, Ithaca, NY 14853, USA

(Received 15 August 2006 and in revised form 10 January 2007)

We investigate aspects of hovering insect flight by finding the optimal wing kinematics which minimize power consumption while still providing enough lift to maintain a time-averaged constant altitude over one flapping period. In particular, we study the flight of three insects whose masses vary by approximately three orders of magnitude: fruitfly (*Drosophila melanogaster*), bumblebee (*Bombus terrestris*), and hawkmoth (*Manduca sexta*). Here, we model an insect wing as a rigid body with three rotational degrees of freedom. The aerodynamic forces are modelled via a quasi-steady model of a thin plate interacting with the surrounding fluid. The advantage of this model, as opposed to the more computationally costly method of direct numerical simulation via computational fluid dynamics, is that it allows us to perform optimization procedures and detailed sensitivity analyses which require many cost function evaluations. The optimal solutions are found via a hybrid optimization algorithm combining aspects of a genetic algorithm and a gradient-based optimizer. We find that the results of this optimization yield kinematics which are qualitatively and quantitatively similar to previously observed data. We also perform sensitivity analyses on parameters of the optimal kinematics to gain insight into the values of the observed optima. Additionally, we find that all of the optimal kinematics found here maintain the same leading edge throughout the stroke, as is the case for nearly all insect wing motions. We show that this type of stroke takes advantage of a passive wing rotation in which aerodynamic forces help to reverse the wing pitch, similar to the turning of a free-falling leaf.

1. Introduction

Insect flight is a metabolically costly endeavour, requiring mass-specific oxygen consumption rates which are about an order of magnitude higher than than those measured in their terrestrially locomoting counterparts (Dickinson & Lighton 1995; Harrison & Roberts 2000). Additionally, flying represents a 50–200 fold elevation from the basal metabolic rate (Kammer & Heinrich 1978; Dudley 2000). Hovering flight is particularly costly, as there is no ambient wind to aid in lift generation. Accordingly, a reasonable hypothesis is that insects move their wings in a manner which minimizes the metabolic cost associated with their motion. In this study, we test this hypothesis for the case of hovering flight and examine its implications through modelling the fluid forces on an insect wing and finding and analysing the optimal kinematics of motion for a given morphology. Specifically, we investigate the optimal kinematics for fruitfly (*Drosophila melanogaster*), bumblebee (*Bombus terrestris*), and hawkmoth (*Manduca sexta*) morphologies. These insects range in mass by approximately three orders of magnitude.

This idea of optimizing traits with respect to some cost function as means of explaining animal behaviour has generated much interest (Alexander 1996, 2001; Srinivasan & Ruina 2006; Wilkening & Hosoi 2006; Parker & Smith 1990) and controversy (Gould & Lewontin 1979) amongst evolutionary biologists and biomechanists. Much of the criticism aimed at studying biomechanics problems in this manner states that given the many functions of a living organism, it is unclear that a specific behaviour can be predicted by optimizing a single function. Moreover, even if such a function can be defined, it is not clear that any new insight must necessarily emerge from the study. However, for the case of a hovering insect, the energetic demands associated with maintaining flight make the power associated with generating a particular wing motion a natural candidate for a cost function. This clear relationship between form and function (wing kinematics and hovering ability) allows us to investigate whether quantitative study can help to explain some common features in the observed wing motions of a diverse set of insects.

In this study, we find and analyse the energy-minimizing kinematics for the three insects mentioned above via a quasi-steady model of fluid forces. This model is similar to the one used by Pesavento & Wang (2004) and Andersen, Pesavento & Wang (2005*a*, *b*), to study the dynamics of a free-falling rigid plate. From this model, we calculate the average lift production and power consumption over the course of a flapping cycle. Using a hybrid optimization algorithm which combines a genetic algorithm with a gradient-based optimizer, we find the kinematics which minimize the power usage while still producing enough lift to maintain hovering flight. Aspects of these kinematics are then compared to previously measured wing strokes. We also study the sensitivity of the optimal solutions to perturbations in various kinematic parameters to gain insight into why the optimal kinematics are at the values found. Finally, we investigate why most insects use a single leading edge throughout a flapping cycle, as opposed to alternating the leading edge near the onset of each half-stroke.

2. Model of insect hovering

Here we describe our mathematical model for calculating the forces, torques, and power consumption associated with insect flight, as well as the computational methods used to analyse it and determine the optimal kinematics.

2.1. *Coordinate definitions and transformations*

We assume that an insect's wing is a rigid plate and is allowed to rotate through each of its three Euler angles. That is, it can rotate azimuthally (ϕ), vertically (θ), and can pitch about its radial axis (η). If z is the vertical direction, y is the forward direction of the insect, and x is perpendicular to the forward direction in the horizontal plane, then we have that

$$\begin{pmatrix} x \\ y \\ z \end{pmatrix} = \begin{pmatrix} r\cos\theta\cos\phi \\ r\cos\theta\sin\phi \\ r\sin\theta \end{pmatrix}. \tag{2.1}$$

This is visualized in figure 1.

As will be seen in § 2.4, the equations for the aerodynamic forces on a section of the wing become simplified if we view the system's velocities in terms of coordinates co-moving with the wing, x' and y' (figure 1). This transformation is achieved by writing the position of the wing slice in spherical coordinates, and then rotating

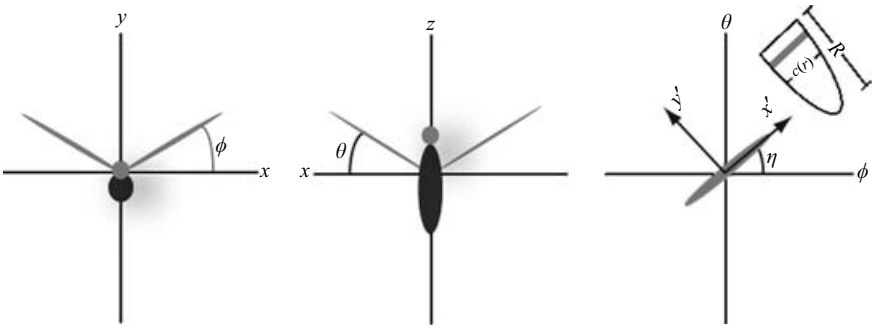

FIGURE 1. Angle definitions.

through the pitching angle, η . In matrix form, this can be written as

$$\begin{pmatrix} \hat{x}' \\ \hat{y}' \end{pmatrix} = \boldsymbol{R}_1 \boldsymbol{R}_2 \begin{pmatrix} \hat{x} \\ \hat{y} \\ \hat{z} \end{pmatrix}, \tag{2.2}$$

where

$$\boldsymbol{R}_1 = \begin{pmatrix} \cos\eta & \sin\eta \\ -\sin\eta & \cos\eta \end{pmatrix} \tag{2.3}$$

and

$$\boldsymbol{R}_2 = \begin{pmatrix} -\sin\phi & \cos\phi & 0 \\ -\sin\theta\cos\phi & -\sin\theta\sin\phi & \cos\theta \end{pmatrix}. \tag{2.4}$$

Using this transformation and differentiating with respect to time, we have

$$v_{x'} = r(\dot{\phi}\cos\theta\cos\eta + \dot{\theta}\sin\eta), \tag{2.5}$$

$$v_{y'} = r(\dot{\theta}\cos\eta - \dot{\phi}\cos\theta\sin\eta), \tag{2.6}$$

$$a_{x'} = r([\ddot{\phi}\cos\theta + \dot{\theta}(\dot{\eta} - \dot{\phi}\sin\theta)]\cos\eta + (\ddot{\theta} - \dot{\eta}\dot{\phi}\cos\theta)\sin\eta), \tag{2.7}$$

$$a_{y'} = r([\dot{\theta}(\dot{\eta} - \dot{\phi}\sin\theta) - \ddot{\phi}\cos\theta]\sin\eta + (\ddot{\theta} - \dot{\eta}\dot{\phi}\cos\theta)\cos\eta), \tag{2.8}$$

where v_i and a_i are the velocity and the acceleration of the wing in direction i, and r is the distance along the radius from the wing's base.

2.2. *Wing geometry*

For simplicity, the wing cross-section along the chord is assumed to be elliptical, with semi-minor axis, b, which represents the wing thickness. The chord length, $c(r)$, of the wing is assumed to vary like a half-ellipse along the wing radius. This is similar to the assumption made in Weis-Fogh (1973). Hence, the chord length as a function of radius is given by

$$c(r) = \frac{4\bar{c}}{\pi}\sqrt{1 - \frac{r^2}{R^2}}, \tag{2.9}$$

where $\bar{c}$ is the mean chord length of a wing and R is the wing's base-to-tip radius. We assume that $b \ll \bar{c}$. Morphological values used in this study were taken from Ennos (1989) for the fruitfly, Dudley & Ellington (1990*a*) for the bumblebee, and Willmott & Ellington (1997) for the hawkmoth.

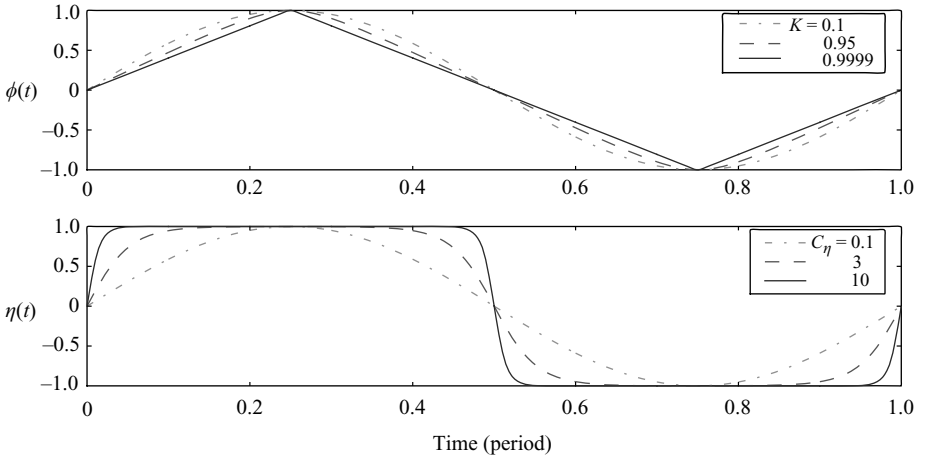

FIGURE 2. Dependence of $\phi(t)$ and $\eta(t)$ on K and C_η.

2.3. *Wing kinematics*

Drawing upon available kinematic data from prior empirical studies (Ellington 1984; Ennos 1989; Dudley & Ellington 1990*a*; Willmott & Ellington 1997; Russell 2004; Fry, Sayaman & Dickinson 2005), the flapping motion of hovering flight is parameterized specifically in order to observe the effects of the rotation speed and relative phases of the wing's pitch and reversal, as well as the frequency and amplitude of the motion in the three angular degrees of freedom described in § 2.1.

The azimuthal coordinate, $\phi(t)$, is given by a smoothed triangular waveform,

$$\phi(t) = \frac{\phi_m}{\sin^{-1} K} \sin^{-1}[K \sin(2\pi f t)], \tag{2.10}$$

where $0 < K < 1$. In the limit where $K \to 0$, $\phi(t)$ becomes sinusoidal, and in the limit of K approaching 1, $\phi(t)$ is a triangular waveform (figure 2). In effect, K can be viewed as a measure of how rapidly the wing reverses direction. This functional form was inspired by comparing the azimuthal kinematics of the experiments listed above, which often found a near-sinusoidal form, and robotic wing experiments, which used a rounded triangular form (Sane & Dickinson 2001).

The angle related to vertical displacement, $\theta(t)$, is described by a sinusoidal oscillation,

$$\theta(t) = \theta_m \cos(2\pi N f t + \Phi_\theta) + \theta_0, \tag{2.11}$$

where N is either 1 or 2: $N = 1$ corresponds to one vertical oscillation per flapping period, and $N = 2$ corresponds to a figure-of-8 motion.

Finally, the pitching coordinate, $\eta(t)$, is described by a periodic hyperbolic function,

$$\eta(t) = \frac{\eta_m}{\tanh C_\eta} \tanh[C_\eta \sin(2\pi f t + \Phi_\eta)] + \eta_0. \tag{2.12}$$

As C_η approaches 0, $\eta(t)$ becomes sinusoidal, and as $C_\eta \to \infty$, $\eta(t)$ tends towards a step function (figure 2). Hence, the value of C_η is inversely related to the duration of wing pitch reversal.

In (2.10)–(2.12), there is a total of 11 parameters which need to be fixed to describe a wing stroke (table 1). Additionally, we assume that the motions of wings are symmetrical about the body. Despite the fact that this parameterization only looks

	Description	Min	Max
f	Frequency	0	∞
ϕ_m	Azimuthal amplitude	0	$\pi/2$
θ_m	Vertical amplitude	0	$\pi/2$
η_m	Pitching amplitude	0	π
θ_0	Vertical offset	$\theta_m - \pi/2$	$\pi/2 - \theta_m$
η_0	Pitching offset	$\eta_m - \pi$	$\pi - \eta_m$
K	Affects the shape of $\phi(t)$	0	1
C_η	Affects the duration of wing rotation	0	∞
N	Multiplier of $\theta(t)$ period	1	2
Φ_θ	Vertical phase offset	$-\pi$	π
Φ_η	Pitching phase offset	$-\pi$	π

TABLE 1. Table of independent model parameters and their constraints.

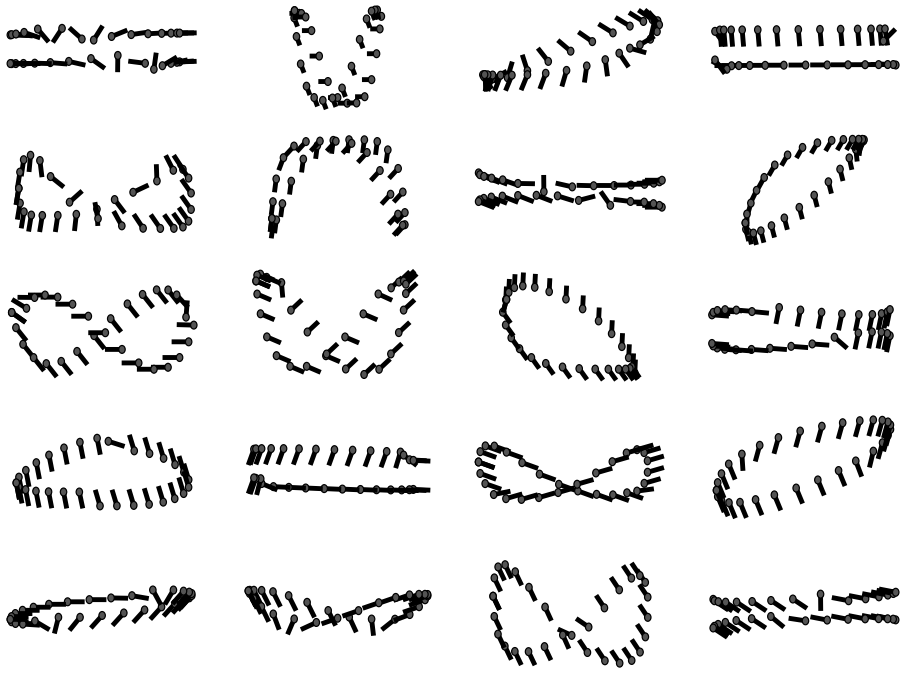

FIGURE 3. A selection of possible wing kinematics. The lines represent a wing chord cross-section, and the dots are placed on the same edge of the wing throughout the stroke.

at a subspace of all possible periodic functions, a wide range of kinematics is still available to the insect, as seen in figure 3.

2.4. *Aerodynamic force model*

The forces acting upon a wing are found via the model formulated to study the motion of a free-falling plate (Pesavento & Wang 2004; Andersen *et al.* 2005*a*) combined with a blade-element assumption that the total force on the wing is the sum of forces on many infinitesimal segments. This is a quasi-two-dimensional force model, as the instantaneous aerodynamic forces for each blade-element are in the plane perpendicular to the wing radius. The utility of this model, as opposed to the vastly more computationally costly method of direct numerical simulation via

computational fluid dynamics, is that it allows us to perform optimization procedures and detailed sensitivity analyses which require many evaluations of the cost function in question.

Specifically, the forces and torque on an infinitesimal slice of the wing are given by

$$\mathrm{d}F_{x'} = \left[\left(\frac{c(r)}{\bar{c}R}M_{wing} + m_{22}\right) v_{y'}\dot{\eta} - \rho_f \Gamma v_{y'} - m_{11}a_{x'}\right]\mathrm{d}r - \mathrm{d}F^{v}_{x'}, \tag{2.13}$$

$$\mathrm{d}F_{y'} = \left[-\left(\frac{c(r)}{\bar{c}R}M_{wing} + m_{11}\right) v_{x'}\dot{\eta} + \rho_f \Gamma v_{x'} - m_{22}a_{y'}\right]\mathrm{d}r - \mathrm{d}F^{v}_{y'}, \tag{2.14}$$

$$\mathrm{d}\tau^{aero}_{\eta} = [(m_{11} - m_{22})v_{x'}v_{y'} - I_a\ddot{\eta}]\,\mathrm{d}r - \mathrm{d}\tau^{v}, \tag{2.15}$$

where a_i is the acceleration component of the wing in coordinate i, M_{wing} is the mass of a wing, $c(r)$ and $\bar{c}$ are the chord length and average chord length as defined in (2.9), R is the wing radius, Γ is the circulation around the wing, $\mathrm{d}F^{v}_{x'}$, $\mathrm{d}F^{v}_{y'}$, and $\mathrm{d}\tau^{v}$ represent the viscous forces and torque on the wing segment, m_{11}, m_{22}, and I_a are added-mass terms, and ρ_f is the density of the surrounding fluid (taken to be $1.29\,\mathrm{kg\,m^{-3}}$). In the two force equations, the first term is due to the fact that the forces are being measured in a rotating coordinate frame, the second term is the force produced via circulation, the third term is an added-mass force, and the final term is the viscous dissipation.

More specifically, the circulation, viscosity, and added-mass term are given by

$$\Gamma = -\tfrac{1}{2}C_T c(r)|\boldsymbol{v}|\sin 2\alpha + \tfrac{1}{2}C_R c^2(r)\dot{\eta}, \tag{2.16}$$

$$\boldsymbol{F}^{v} = \tfrac{1}{2}\rho_f c(r)\left[C_D(0)\cos^2\alpha + C_D(\pi/2)\sin^2\alpha\right]|\boldsymbol{v}|\langle v_{x'}, v_{y'}\rangle\,\mathrm{d}r, \tag{2.17}$$

$$\mathrm{d}\tau^{v} = \tfrac{1}{16}\pi\rho_f c^4(r)[\mu_1 f + \mu_2|\dot{\eta}|]\dot{\eta}\,\mathrm{d}r, \tag{2.18}$$

$$m_{11} = \tfrac{1}{4}\pi\rho_f b^2, \quad m_{22} = \tfrac{1}{4}\pi\rho_f c^2(r), \quad I_a = \tfrac{1}{128}\pi\rho_f[c^2(r) + b^2]^2. \tag{2.19}$$

Here, α is the angle of attack, C_T and C_R are, respectively, the translational and rotational lift coefficients of the wing, $C_D(\alpha)$ is the wing's drag coefficient as a function of the angle of attack, μ_1 and μ_2 are dimensionless coefficients related to the viscosity of the fluid, and f is the flapping frequency. Values for C_T, $C_D(0)$, and $C_D(\pi/2)$ for fruitfly and hawkmoth wings were taken from model flapping experiments (Dickinson, Lehmann & Sane 1999; Usherwood & Ellington 2002). Bumblebee measurements were taken from wind tunnel measurements in Dudley & Ellington (1990*b*). Finally, it is also possible to obtain analytic expressions for the components of the aerodynamic torques in the $\hat{\phi}$- and $\hat{\theta}$-directions through

$$\tau^{aero}_{i} = \int_{r=0}^{r=R} (\boldsymbol{r} \times \mathrm{d}\boldsymbol{F})_i. \tag{2.20}$$

For the calculations presented here, the torques and forces are analytically calculated at 1000 evenly spaced time steps over a single period and average forces and torques are obtained at via numerical integration.

The total lift on the wing is calculated by transforming the force vectors back into the laboratory frame, in which $\hat{z}$ is the unit vector in the vertical direction. F_z is defined as the magnitude of the $\hat{z}$ component of the total force. In order to make a convenient non-dimensional measure of the vertical force on an insect, we will

subsequently quantify an insect's lift by L, which is defined as

$$L \equiv \frac{2\langle F_z \text{ From One Wing}\rangle}{mg}, \tag{2.21}$$

where m is the total weight of the insect and $g = 9.81\,\mathrm{m\,s^{-2}}$. Hence, if $L \geqslant 1$, the insect is able to produce enough lift to fly.

2.5. *Modelling power consumption*

Given a particular morphology and set of kinematics, we also wish to determine the amount of power necessary to produce the desired wing motion. We assume that the energetic cost to the insect is given by the time-averaged positive mechanical power output. This includes both the power necessary to overcome aerodynamic drag and the inertial power required to accelerate the wing's inertia. Additionally, we assume that the cost for negative power is negligible and that the effect of elastic storage, which has been measured to be on the order of 10 %, is minimal (Dickinson & Lighton 1995).

We model the power consumption by assuming that motions are powered by rotational actuators located at the base of the wing. Using the Eulerian equations for the rotational motion of a rigid body and given the assumptions made above, we have that the power output from rotation through angle i (p_i) is given by

$$p_i(t) = \Omega_i\left[I_i\dot{\Omega}_i - \Omega_j\Omega_k(I_j - I_k) - \tau_i^{aero}\right], \tag{2.22}$$

where $[i, j, k]$ is a cyclic permutation of $[\phi, \theta, \eta]$, I_i is the moment of inertia when rotating in i, and Ω_i is the angular velocity in the respective angular coordinate. The first two terms of (2.22) represent the power output the wing must overcome in order to move in a vacuum, whereas the final term (using the definition of τ^{aero} from (2.15) and (2.20)) is the additional power that must be added in order to overcome aerodynamic forces. This equation implies perfect elastic storage because whenever $p_i < 0$, it counts as negative power, meaning that when the wing decelerates, energy is put into the system to be used later when it accelerates. In order to only take positive power into account, we define $P_i(t)$, the positive power consumption necessary to move the wing through angle i, by

$$P_i(t) = \Xi[p_i(t)] \tag{2.23}$$

where $\Xi(x)$ is defined by

$$\Xi(x) = \begin{cases} x & \text{if } x > 0 \\ 0 & \text{if } x \leqslant 0. \end{cases} \tag{2.24}$$

The total mass-normalized power required to perform the wing motion, P^*, is then given by

$$P^* = \frac{P_\phi + P_\theta + P_\eta}{\text{insect mass}}. \tag{2.25}$$

2.6. *Model validation*

To test the compatibility of our model with results obtained from three-dimensional Navier–Stokes simulations, we look at the cases of a fruitfly, a bumblebee, and a hawkmoth flying with a horizontal stroke plane ($\theta_m = \theta_0 = 0$) and a sinusoidally varying azimuthal angle (corresponding to $K \to 0$ in (2.10)). Here, we utilize the same morphological and kinematic data as Sun & Du (2003) in order to compare results (table 2). As mentioned in § 2.4, C_T, $C_D(0)$, and $C_D(\pi/2)$ are obtained by fitting lift and drag coefficient data from previous empirical studies (Dickinson *et al.* 1999;

Insect	M (mg)	M_{wing} (mg)	R (mm)	$\bar{c}$ (mm)	I_{wing} (g cm^2)
Fruitfly	0.72	8.6×10^{-4}	2.02	0.67	0.80×10^{-8}
Bumblebee	175	0.46	13.2	4.02	0.17×10^{-3}
Hawkmoth	1648	47	51.9	18.26	0.184
Insect	f (Hz)	ϕ_m (deg.)	C_T	$C_D(0)$	$C_D(\pi/2)$
Fruitfly	254	75°	1.833	0.21	3.35
Bumblebee	116	58°	1.341	0	2.93
Hawkmoth	26.3	60.5°	1.678	0.07	3.06

TABLE 2. Morphological and kinematic parameters used for optimization and validation.

Insect	Quantity	Quasi-Steady	CFD (Sun & Du)
Fruitfly	L	1.003	1.0
	P^*	24	30
Bumblebee	L	0.95	1.0
	P^*	53	56
Hawkmoth	L	1.15	1.0
	P^*	44	46

TABLE 3. Comparison between quasi-steady and CFD (P^* in units of W kg^{-1}).

Usherwood & Ellington 2002; Dudley & Ellington 1990*a*) to the forms $C_L(\alpha) = C_T \sin(2\alpha)$ and $C_D(\alpha) = C_D(0)\cos^2\alpha + C_D(\pi/2)\sin^2\alpha$ from (2.16)–(2.17). It should be noted that these measurements are based on experiments involving dynamically scaled models of the wings. As in Andersen *et al.* (2005*a*), C_R is set to be equal to π for all three insects. The mid-stroke angle of attack, α_m, is chosen to have the values 44°, 28°, and 32° for the fruitfly, bumblebee, and hawkmoth, respectively, used in Sun & Du (2003) for the sake of comparison. Finally, the non-dimensional viscous torque parameters, μ_1 and μ_2, are both set to be equal to 0.2, which was taken from Andersen *et al.* (2005 *b*) for cases at similar Reynolds numbers. The values of μ_1 and μ_2 have a small effect on the total power, largely resulting from the fact that the power required to overcome translational drag dominates the power required to overcome viscous torque. They were both tested in the range [0, 20], resulting in less than 1 % change in both lift production and power consumption. Additionally, since Sun & Du (2003) assume that the contribution of rotational power is negligible, P_η is taken to be 0 for this section of the paper only.

As seen in table 3, the quasi-steady model agrees with the CFD calculations to within approximately 15 %. For the fruitfly, L is predicted almost exactly, but the specific power, P^*, is slightly underestimated. In the case of the hawkmoth, though, the specific power agrees well with the CFD calculation and the amount of lift predicted is off by about 15 %. For the bumblebee, both the lift and power agree well with the CFD results.

2.7. *Optimization*

Given the model of forces and biomechanics described in the previous sections, we optimize the kinematic parameters listed in table 1 in order to minimize the mass-specific power output of an insect (P^*) with a fixed morphology. This is a nonlinear optimization process with the constraint that $L \geqslant 1$. The problem also is constrained

by the physical limitations on the parameters listed in table 1 (i.e. $0 \leqslant \phi_m \leqslant \pi/2$). This constrained optimization was converted into a more tractable problem by defining the fitness, F, corresponding to parameter set Υ, by

$$F = P^* + r\Theta(1-L) + s\sum_{j\in\Upsilon}\frac{|\zeta_j|}{\mathrm{Max}_j - \mathrm{Min}_j} \tag{2.26}$$

where $\Theta(x)$ is the Heaviside step function, ζ_j is the distance that parameter j is outside the range specified by Max_j and Min_j given in table 1, and r, s are positive, real parameters which specify the strength of the penalty for violating the lift and physical constraints, respectively. For the optimizations to follow, we use $r = s = 2000$.

The procedure used here is a hybrid of the clustering genetic algorithm (GA) used in Milano & Koumoutsakos (2002) for other fluid dynamics applications and a Powell simplex algorithm (Powell 1970) for local optimization at the end. The GA is started with a population of 200 parameter sets which are then evolved to be grouped in a globally minimal basin. The initial sets are randomly chosen from all possible sets within the range allowed by the values in table 1 in order to avoid biasing. After narrowing the population sufficiently, the simplex algorithm was used to relax each of the parameter sets found via the GA to the local optimum of the basin. All of the results to follow are validated by multiple runs of the algorithm, each of which matched to within the tolerance set for the simplex algorithm (relative tolerances of 10^{-10} for the fitness function and all parameters).

3. Optimization results

3.1. *Optimized kinematics*

Wing kinematics, force production, and power consumption resulting from the three optimizations are shown in figure 4. Data from the optimizations are listed in tables 4 and 5. For the fruitfly, the optimal wing motion is largely flat but slightly U-shaped, qualitatively similar to the observed kinematics (Ennos 1989; Fry *et al.* 2005). Additionally, the force production and power consumption are relatively constant along the mid-stroke, dropping off precipitously during wing rotation. For both the bumblebee and hawkmoth motions, however, we see a figure-of-8 motion with a larger stroke deviation ($\sim 10^\circ$) and less constant forces and powers during the mid-stroke. The latter effect is especially pronounced for the power consumption.

Additionally, the frequencies of the optimized kinematics are similar to the observed values. For the fruitfly, the optimized frequency of 234 Hz is within the measured range of 210–260 Hz seen in empirical studies (Ennos 1989; Fry *et al.* 2005). For the two larger insects, although the optimized frequencies are slower than the observed values, there still exists a reasonable agreement between the optimization and empirical data. Speifically, the optimized hawkmoth motion has a frequency of 19 Hz (observed range: 24–26 Hz (Willmott & Ellington 1997), and the optimized bumblebee frequency is 122 Hz (observed range: 145–155 Hz (Dudley & Ellington 1990*a*)).

Finally, for all three insects, the optimal motions are such that they produce nearly exactly enough lift to hover, and not more (to within $mg \times 10^{-15}$). Since additional lift production requires an increase in power consumption, the inequality constraint placed upon the optimization acts more like an equality constraint ($L \equiv 1$ as opposed to $L \geqslant 1$). More will be said about this later.

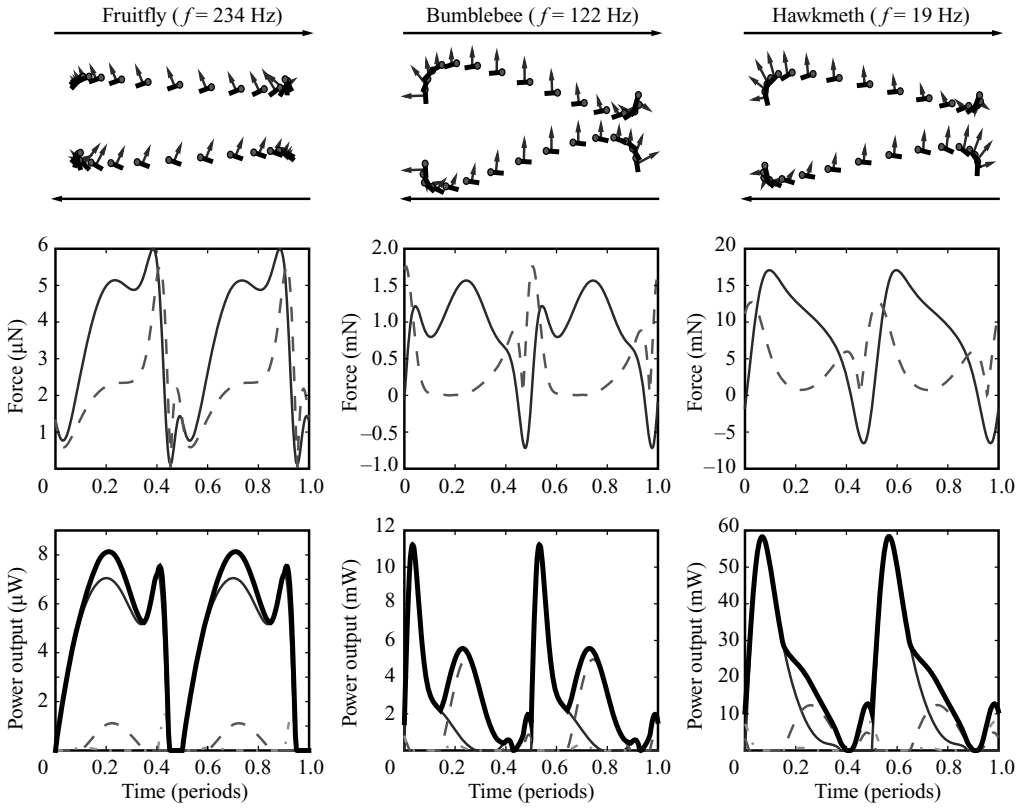

FIGURE 4. Kinematics, forces, and power for optimized wing motions. Top: the motion of the wing chord with dots representing the wing's leading edge. The arrows are the instantaneous forces on the wing. Middle: the vertical forces (solid line) and the magnitude of horizontal (dashed line) forces on the wing over one flapping period. Bottom: the total power output (thick solid line) and its three components: P_ϕ (thin solid line), P_θ (dashed), and P_η (dot-dashed).

	Fruitfly	Bumblebee	Hawkmoth
f (Hz)	234	122	19
ϕ_m (deg.)	90.0	90.0	90.0
θ_m (deg.)	3.1	12.3	8.1
η_m (deg.)	72.7	87.0	85.3
θ_0 (deg.)	−0.65	1.83	2.67
η_0 (deg.)	90.0	−90.0	−90.0
K	0.704	0.925	0.796
C_η	2.375	1.223	0.711
N	2	2	2
Φ_θ (deg.)	−70.6	−102.2	−109.2
Φ_η (deg.)	−72.4	−91.8	−97.9

TABLE 4. Optimal parameters.

3.2. *Kinematics with constrained stroke amplitudes*

A possible explanation for the optimized frequencies being consistently lower than the observed values lies in the fact that for all three optimizations, the stroke amplitude,

	Fruitfly	Bumblebee	Hawkmoth
$L-1$	2.9×10^{-15}	2.5×10^{-16}	6.4×10^{-16}
$\langle F_z\rangle/\langle Drag\rangle_{rms}$	1.80	1.94	1.58
$\langle P^{Aero}\rangle/\langle P^{Inertial}\rangle$	3.74	.53	1.25
$P^*(\mathrm{W\,kg^{-1}})$	14.6	39.2	26.6

TABLE 5. Optimization results.

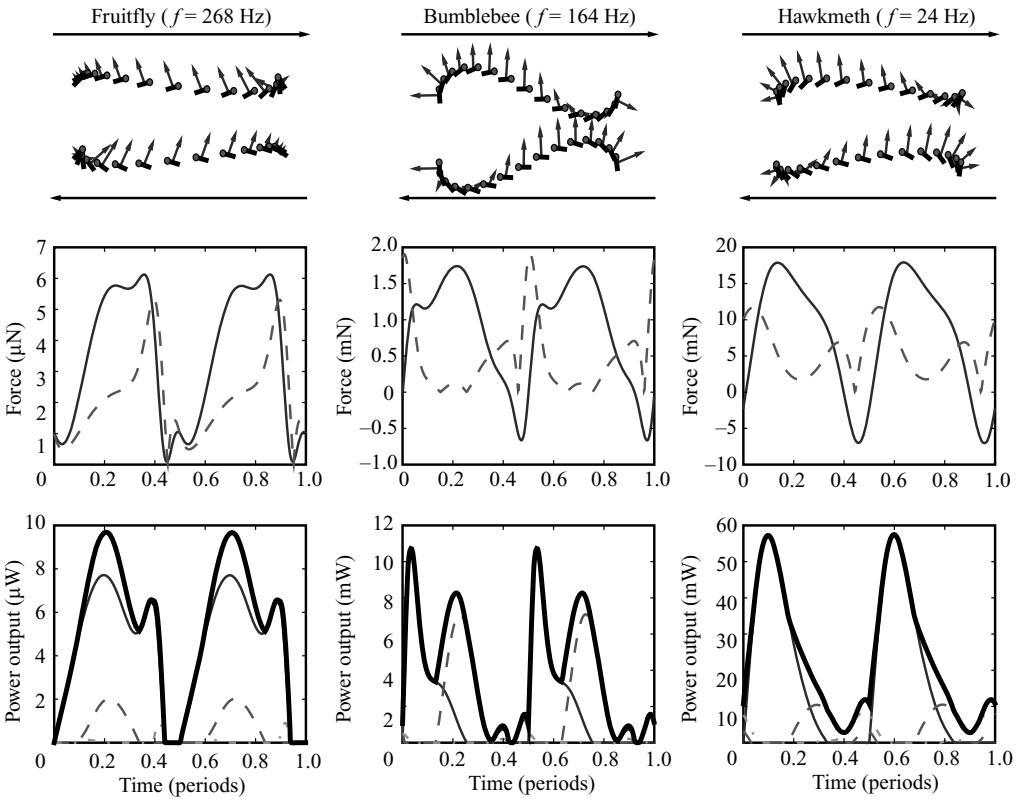

FIGURE 5. Kinematics, forces, and powers for optimized wing motions with constrained ϕ_m (layout is the same as in figure 4).

ϕ_m, is at the maximum allowed value of 90°. Intuitively, this makes sense, as a larger stroke amplitude allows a larger percentage of the period to be spent in the mid-stroke, where most of the lift is generated. Hence, this additional generation of lift per period allows a slower flapping frequency. Insects, however, are limited by additional constraints which do not exist in our model. In particular, the cost for moving the wing is likely to be a non-constant function of the stroke position (i.e. the cost required to move a wing from $\phi=-15°$ to $\phi=15°$ is different than the cost to move from $\phi=60°$ to $\phi=90°$). Hence, it is of interest to observe the wing motions that result from optimizing the kinematics while keeping ϕ_m fixed to the empirically observed value (75° for the fruitfly, 58° for the bumblebee, and 60.5° for the hawkmoth).

Results from this optimization are shown in figure 5. For all three insects, the decrease in ϕ_m results in a higher flapping frequency, as expected. Specifically, the

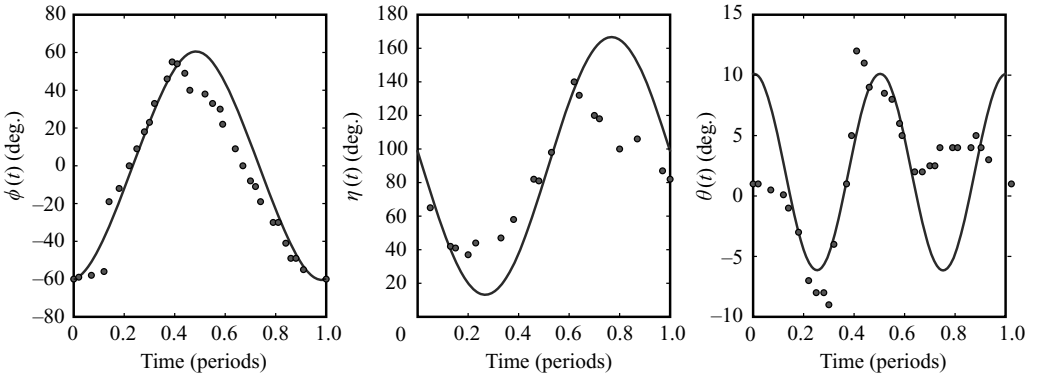

FIGURE 6. Comparison between optimized (solid line) hawkmoth hovering kinematics and observed data (dots) from Willmott & Ellington (1997).

frequencies resulting from this optimization with a constrained stroke amplitude were 268 Hz for the fruitfly, 164 Hz for the bumblebee, and 24 Hz for the hawkmoth. Each of these values is within or only slightly above the empirically observed range of frequencies. Also, it should be noted that although small changes exist between the other stroke parameters, the wing motions, forces, and powers resulting from optimizing with a constrained stroke amplitude do not differ qualitatively from the non-constrained case. In particular, for the case of the hawkmoth (figure 6), we see good agreement between the optimized solution and the wing stroke empirically observed by Willmott & Ellington (1997). The primary disagreements between the optimized and the observed strokes occur due to the lack of asymmetry in our kinematic equations. However, for all three angles, there is quantitative agreement for the amplitudes, phases, and the frequency, of the motion.

4. Sensitivity of optimal solutions

Given the optimized kinematics presented in figure 4 and table 4, we now investigate the effects of perturbing various parameters on their lift and power production. This is done to gain insight into why these particular parameters are optimal, as well as to understand more fully the structure of the optimal basin. Figure 7 shows the dependence of L and P^* for each of nine parameters for the hawkmoth, assuming all the other parameters remain constant at their optimized values. Only the hawkmoth analyses are shown here owing to the qualitative similarity between the sensitivity analyses of all three of the insects studied here.

We see from these single-variable sensitivity analyses that although interplay exists between the parameters, the location of the optimal value can be explained by only three categories of behaviour. The first category contains parameters where a conflict between lift production and power consumption affects the optimal value. These three parameters (ϕ_m, θ_m, and η_m, figure 7*a–c*) are the amplitudes in the three angular degrees of freedom. For the first two cases of ϕ_m and θ_m, an increased amplitude corresponds to more lift production, but also results in strokes which require more power. Hence, given our optimization's constraint that $L \geqslant 1$, the optimal values for these parameters will be set by finding the minimal value where $L = 1$. This helps to explain the result in § 3.1 where the inequality constraint of our optimization becomes an equality constraint. Any deviation from the manifold where $L = 1$ would result in either a violation of the lift constraint or an increase in power consumption.

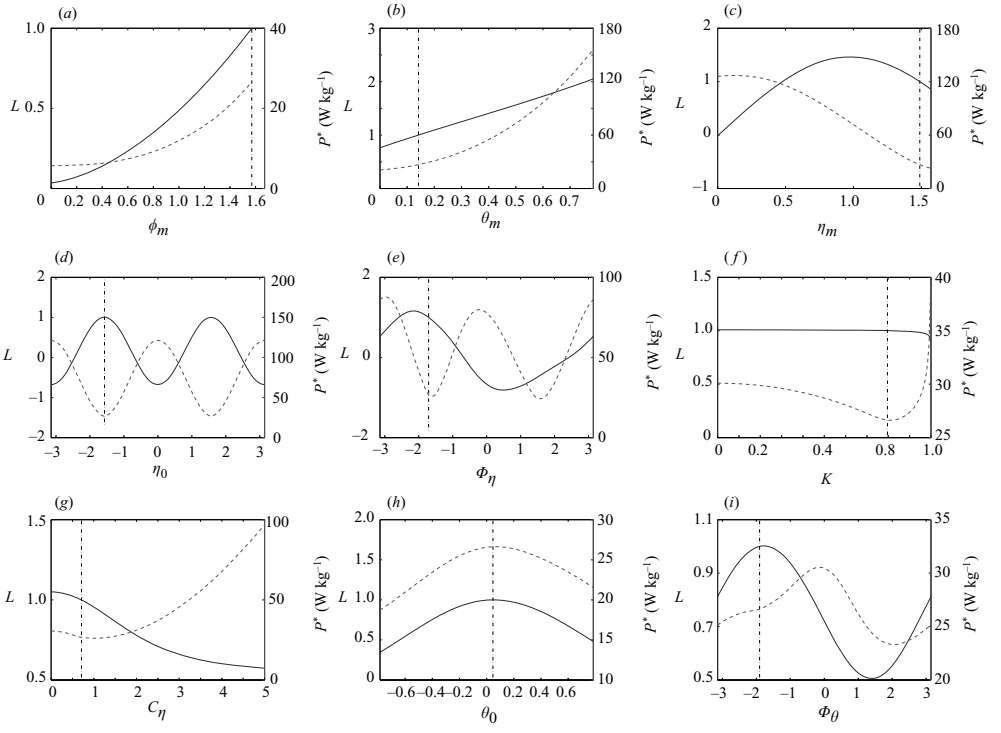

FIGURE 7. Single-parameter sensitivity analyses for the hawkmoth. The solid lines show L as a function of the given parameter, and the dashed lines represent the variation of P^*. The dot-dash vertical lines indicate the position of the optimal solution for the parameter in question.

Similarly, for η_m, we see that for large values of the amplitude (corresponding to small mid-stroke angles of attack), both the lift and power decrease monotonically. Hence, the optimal value of η_m is the largest value such that the lift constraint is met.

The second category contains parameters where the optimized value is at or near the global minimum with respect to P^* (namely, η_0, C_η, Φ_η, and K, figure 7*d–g*). Variations away from the optimum in these parameters tend to cause significant increases in power consumption. The exception to this is K, but the optimal value is the global minimum in P^* due to the relative flatness of the dependence of L on the parameter. It also should be noted that all four of these parameters are directly related to the speed and phase of wing rotation.

The final category of parameters is those where L is maximized irrespective of power consumption (θ_0 and Φ_θ, figure 7*h*, *i*). For these parameters, both related to $\theta(t)$, the relatively small effect they have on P^* gives more importance to providing a maximal amount of lift.

5. Rotational power and passive wing rotation

An interesting feature of the optimized kinematics is that the cost of pitching the wing corresponds to only a small fraction of the total power consumption (1.4 % for the fruitfly, 4.5 % for the bumblebee, and 5.6 % for the hawkmoth). In particular, the optimal kinematics are such that the stroke maintains a constant leading edge throughout a flapping period, as opposed to switching the leading edge during wing

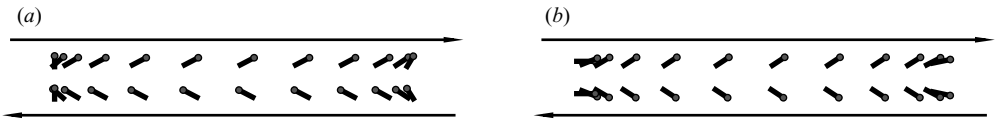

FIGURE 8. Examples of wing kinematics with differing wing rotation strategies: (*a*) constant leading edge, (*b*) alternating leading edge.

rotation (figure 8). This observation matches empirically observed results for nearly all insects. Previously, the use of a single leading edge was assumed to occur for structural (as opposed to aerodynamic) reasons, as the leading edge of the wing must be relatively thick compared to the trailing edge, since the additional fluid forces which occur at the trailing edge lead to greater stress on that portion of the wing (Norberg 1972). Hence, a wing can be lighter if only one of its edges needs to be made of the thicker material that a leading-edge side requires. Our model, however, assumes a symmetry between the two edges of the wing. Hence, the fact that the wing keeps the same leading edge through the optimization implies that there is another reason for this rotation. What appears to occur is a passive–dynamic relationship between the inertial forces required to flip the wing over and the fluid forces acting on the wing during rotation. This effect is seen in figure 7(*d*), where both maximum lift production and minimum power consumption occur at values where the stroke maintains a constant leading edge ($\eta_0 = \pm\pi/2$). Conversely, the lift is minimized and the power maximized at $\eta_0 = 0$, corresponding to an alternating leading edge.

The sensitivity analysis, however, is not a full explanation for the optimal solution using a single leading edge, as the interplay between different parameters may allow more efficient strokes with alternating leading edges. To gain a better understanding, we run the optimization described in § 2.7 but with the additional constraint that the leading edge must switch at some point during the stroke. In other words, for every flapping period, there exist times t_1 and t_2 such that $\boldsymbol{v}(t_1)\cdot\boldsymbol{c}(t_1) < 0 < \boldsymbol{v}(t_2)\cdot\boldsymbol{c}(t_2)$ where $\boldsymbol{v}(t)$ is the velocity vector at time t and $\boldsymbol{c}(t)$ points in the direction of the chord.

Performing this optimization (figure 9), we observe that maintaining a constant leading edge results from the interplay between inertial and aerodynamic powers. Specifically, the two powers largely cancel each other for the case of a single leading edge, whereas they are additive in the case of the optimal kinematics for alternating edges. The amount of power necessary for rotation increases by factors of 190 %, 88 %, and 76 % for fruitfly, bumblebee, and hawkmoth, respectively, when an alternating leading edge is mandated. These differences in efficiency can be explained by the timing of the aerodynamic forces acting on the wing. For a single leading edge, the aerodynamic torque facilitates the turning at the onset of rotation – the fluid is doing work on the wing. For the case of alternating leading edges, however, the wing must do work on the fluid while the wing attempts to accelerate and also does work on the fluid while it decelerates. An energetic benefit exists on neither the onset nor the resolution of rotation, resulting in the increased power consumption observed in figure 9.

6. Summary

We have found and analysed the optimal wing kinematics for the hovering flight of three insects of widely varying masses through the use of a quasi-steady model of fluid forces on a thin plate and a hybrid optimizing algorithm. These solutions minimize power consumption while still producing enough lift to sustain hovering

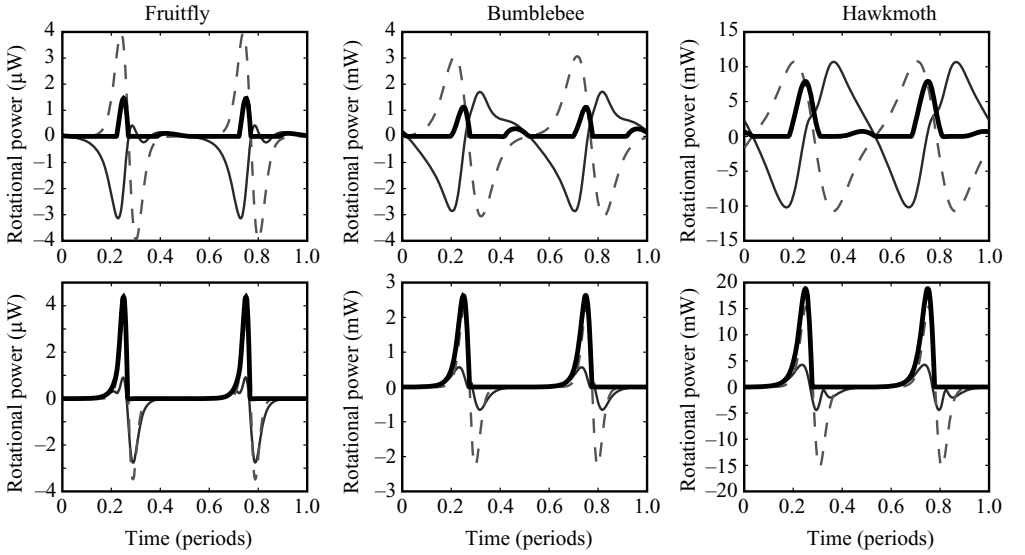

FIGURE 9. Rotational power output for optimized wing motions: the rotational power necessary to pitch the wing for an optimized stroke with either a single (top) or alternating (bottom) leading edge for the three insects. The thick solid line is the total rotational power consumption (P_η), the thin solid line represents the aerodynamic power, and the dashed line is the inertial power. The kinematics from the top three plots are identical to those in figure 4, whereas the kinematics in the bottom plots were generated by running the optimization procedure with the added caveat that the leading edge is forced to switch at some point during the stroke.

flight. We found that these kinematics capture several qualitative aspects of observed flight and predict the observed flapping frequencies well. These agreements become more striking if we fix a parameter by constraining the stroke amplitude, ϕ_m, to its empirically observed value. We also have performed sensitivity analyses of the optimal solutions. From these analyses, we determined the import and effect of varying the kinematic parameters in our model. Finally, we observed that the optimal motions used a single leading edge throughout the stroke, as opposed to alternating edges during wing rotation. Previously thought to occur for purely structural reasons, we found that maintaining a constant leading edge is advantageous due to an interplay between inertial and aerodynamic power. Future work will involve studying the problem from more of a dynamics perspective, investigating not only the interaction between an insect's wings and the surrounding fluid, but also coupling these objects to the motion of the body.

This work was supported by the NSF, AFOSR, and the Packard Foundation.

REFERENCES

ALEXANDER, R. MCN. 1996 *Optima for Animals*. Princeton University Press.

ALEXANDER, R. MCN. 2001 Design by numbers. *Nature* **412**, 591.

ANDERSEN, A., PESAVENTO, U. & WANG, Z. J. 2005*a* Unsteady aerodynamics of fluttering and tumbling plates. *J. Fluid Mech.* **541**, 65–90.

ANDERSEN, A., PESAVENTO, U. & WANG, Z. J. 2005*b* Analysis of transitions between fluttering, tumbling and steady descent of falling cards. *J. Fluid Mech.* **541**, 91–104.

Dickinson, M. H., Lehmann, F.-O. & Sane, S. P. 1999 Wing rotation and the aerodynamic basis of insect flight. *Science* **284**, 1954–1960.

Dickinson, M. H. & Lighton, J. R. B. 1995 Muscle efficiency and elastic storage in the flight motor of *Drosophila*. *Science* **268**, 87–90.

Dudley, R. 2000 *The Biomechanics of Insect Flight*. Princeton University Press.

Dudley, R. & Ellington, C. P. 1990*a* Mechanics of forward flight in bumblebees. i. kinematics and morphology. *J. Expl Biol.* **148**, 19–52.

Dudley, R. & Ellington, C. P. 1990*b* Mechanics of forward flight in bumblebees. ii. quasi-steady lift and power requirements. *J. Expl Biol.* **148**, 53–88.

Ellington, C. P. 1984 The aerodynamics of hovering insect flight. *Phil. Trans. R. Soc. Lond.* B **305**, 1–181.

Ennos, A. R. 1989 The kinematics and aerodynamics of the free flight of some diptera. *J. Expl Biol.* **142**, 49–85.

Fry, S. N., Sayaman, R. & Dickinson, M. H. 2005 The aerodynamics of hovering flight in *Drosophila*. *J. Expl Biol.* **208**, 2303–2318.

Gould, S. J. & Lewontin, R. C. 1979 The spandrels of san marco and the panglossian paradigm: A critique of the adaptionist programme. *Phil. Trans. R. Soc. Lond.* B **205**, 581–598.

Harrison, J. F. & Roberts, S. P. 2000 Flight respiration and energetics. *Annu. Rev. Physiol.* **62**, 179–205.

Kammer, A. E. & Heinrich, B. 1978 Insect flight metabolism. *Adv. Insect Physiol.* **13**, 133–228.

Milano, M. & Koumoutsakos, P. 2002 A clustering genetic algorithm for cylinder drag optimization. *J. Comput. Phys.* **175**, 79–107.

Norberg, R. A. 1972 The pterostigma of insect wings an inertial regulator of wing pitch. *J. Comput. Physiol.* A **81**, 9–22.

Parker, G. A. & Smith, J. M. 1990 Optimality theory in evolutionary biology. *Nature* **348**, 27–33.

Pesavento, U. & Wang, Z. J. 2004 Falling paper: Navier-stokes solutions, model of fluid forces, and center of mass elevation. *Phys. Rev. Lett.* **93**, 144501–144504.

Powell, M. J. D. 1970 A new alogorithm for unconstrained minimization. In *Nonlinear Programming* (ed. J. B. Rosen, O. L. Mangasarian & K. Ritter), pp. 31–66. Academic Press.

Russell, D. B. 2004 Numerical and experimental investigations into the aerodynamics of dragonfly flight. PhD thesis, Cornell University.

Sane, S. P. & Dickinson, M. H. 2001 The control of flight force by a flapping wing: Lift and drag production. *J. Expl Biol.* **204**, 2607–2626.

Srinivasan, M. & Ruina, A. 2006 Computer optimization of a minimal biped model discovers walking and running. *Nature* **439**, 72–75.

Sun, M. & Du, G. 2003 Lift and power requirements of hovering insect flight. *Acta Mechanica Sinica* **19**, 458–469.

Usherwood, J. R. & Ellington, C. P. 2002 The aerodynamics of revolving wings: I. model hawkmoth wings. *J. Expl Biol.* **205**, 1547–1564.

Weis-Fogh, T. 1973 Quick estimates of flight fitness in hovering animals. *J. Expl Biol.* **59**, 139–230.

Wilkening, J. & Hosoi, A. E. 2006 Shape optimization of swimming sheets. *J. Fluid Mech.* (submitted).

Willmott, A. P. & Ellington, C. P. 1997 The mechanics of flight in the hawkmoth *Manduca sexta*. *J. Expl Biol.* **200**, 2705–2745.